ISSN No:-2456-2165

Ca-Markov Model for Simulating Land use Land Cover Dynamics in Rufiji Delta of Tanzania

Job Asheri Chaula
School of Earth Science, Real Estate, Business and Informatics
Department of Computer Systems and Mathematics
Ardhi University-Tanzania

Abstract:- Sustainable management and resilience of ecosystems and their different services from land, water, biodiversity and forests has been highlighted as a means to address environmental degradation in Tanzania. On contrary, there is in adequate information to aid sustainable management of fragile natural resources such as Rufiji Delta. To address the limitation this research was carried out using Landsat data for appraising and simulating the future situation of Rufiji Delta using CA-Markov model. Maximum Likelihood Classification algorithm in ERDAS Imagine software was used for Landsat image classification and accuracy assessment for year 1998, 2008 and 2018 while Ca-Markov model of IDRIS Selva software was used for quantification of LULC change and simulation, correspondingly. The classification results of four different study periods have depicted the quantity land use land cover status in year 1998, 2008 and 2018. In year 1998 the impervious land cover was the largest class with 53413.40 ha (35.74% composition), followed by water bodies with 42506.10 ha (28.44% composition) while mangrove forest and non-mangrove vegetation consisted of 38060.40 ha (25.47 % composition) and 15468.50 ha (10.35% composition), correspondingly. In year 2018 the impervious land cover increased to 60759.70 ha (40.66% composition) while mangrove forest and non-mangrove vegetation consisted of 35062.2 ha (23.46% composition) and 23019.2 ha (15.40% composition), correspondingly. Water bodies declined to 30607.10 ha (20.48% composition) following the consumption of water in hydro-electrical and agricultural expansion proximal to the Rufiji Delta. In year 2048 a notable decline to about 29757.07 ha, (18.91%), 34891.44 ha (21.35were recorded for mangrove forest and water bodies, correspondingly. The ongoing harvesting and clearing of mangrove forest for construction and other local use purpose. Substantial increase in area non-mangrove vegetation and impervious land cover was estimated to 22507.20 ha and 62292.84 ha, correspondingly. Agro afforestation, forestry farming, Agro-Zonation, adoption of AFOLU and LULCF programs are highly recommended in area proximal to Rufiji Delta.

Keywords:- *LULC Dynamics; Simulation Of LULC; LULC Modelling.*

I. INTRODUCTION

Land Cover Land Use (LULC) simulation models are tools to support the analysis of the causes and consequences of land use changes in order to better understand the functioning of the land use system and to support land use planning and policy (Ganasri *et al.,* 2013). LULC simulation models supports exploration of future LULC changes under different scenario conditions (Verburg *et al.,* 2004). A number of the LULC models are available and have been used for unravelling the complex relationships in changing LULC systems and provides insights into the extent and location of LULC change (Houet *et al.* 2007 & Zhigang *et al.* 2011). Land Change Modeller (LCM) and CA-Markov model are among free available LULC simulation models which have been used for unravelling the complex relationships while providing the insights into the extent and location of LULC change.

The LCM is an integrated software module in IDRISI Selva software environment that performs land change analysis, change prediction, and habitat and biodiversity impact assessment (Province, 2016; Mishra *et al.,* 2014). The LCM is embedded in the IDRISI software where only thematic raster images with the same land cover categories listed in the same sequential order can be input for LULC analysis (Megahed *et al*., 2015). LCM evaluates land cover changes between two different times, calculates the changes, and displays the results with various graphs and maps (Province, 2016; Mirhosseini *et al.,* 2016). In the LCM model, a set of tools is included for the rapid assessment of LULC change, hence allowing for one-click evaluation of gains and losses and net change of LULC types, mapping spatial trend of LULC changes both in map and graphical form (Hamdy *et al.* 2017; Mirhosseini *et al.*, 2016).

On the other hand, the CA-Markov Model operates using the outputs of Markov chain and CA model whereby the Markov chain is used for prediction of LULC dynamics and CA model adds spatial characteristics to the predicted LULC. A Markov chain model is applied when describing a process with set of states such as $X = \{X_0, X_1, X_2 \ldots\ldots X_n\}$ and the states successively moves from one state to another state (Ma *et al.,* 2012). The Markov chain is uses a pair of LULC maps from between period-1 and period-2 to analyse and outputs a transition probability matrix, a transition areas

matrix, and a set of conditional probability images. The transition probability matrix is a text file that records the probability that each land cover category will change to every other category (Eastman, 2012). While a transition areas matrix is a text file with records of the number of pixels expected to change from one LULC category to another LULC category at specified number of time units (Paul, 2013). On the other hand, the conditional probability images account the probability that each LULC category would be found at each pixel after the specified number of time units and are calculated as projections from the later of the two input LULC maps (Weng, 2002 & Eastman, 2012). The basic hypothesis of Markov Chain prediction is that future land use at time (t+1), Xm is a function of current land use at time t, Xt (Paul, 2013) and mathematically expressed as in Equation (1).

$$\mathbf{X_{t+1} = f\,(X_t)}\text{……..Equation 1}$$

State of a Markov chain at time t is the value of X_t while the state space of a Markov chain, S is the set of values that each Xt can take. In the Markovian system, the future state of a land use system is modelled on the basis of the immediate proceeding state (Araya & Cabral, 2010). Markov chain is mostly applied to a system which has a finite number of states and that the system undergoes changes from state to state with a probability for each distinct state transition that depends solely upon the current state (Yasmine *et al.*, 2015). The Markov Chain model is a unique and widely used tool in land use modelling which demonstrates the LULC changes as a stochastic process (Weng, 2002). By considering, a system with "n" distinct states undergoes state changes which are strictly Markov in nature, and then the probability that its current state is *"i"* given that its previous state was *"j"* is the transition probability, "P_{ij}". Subsequently, n x n matrix "P" whose ij^{th} element is "P*ij*" is termed the transition matrix of the Markov chain. In Markov chain, the state of the system in future (X_{i+1}) is determined using the former state, X*i* (Ma *et al.* 2012) and does not depend on the current state. Mathematically, the relationship is described using equation (2 and 3).

$$\boldsymbol{Xi}+\mathbf{1}=\boldsymbol{PXi}\text{……..} \text{ Equation 2}$$

Where X_{i+1}, is future state of the system while X*i*, is the former state of the system and P is the transition probability matrix. In Equation (3) a Markov transition probability matrix P, describes the probabilities motion of a population between various states. The individual elements of the matrix reflect the probability that a population moves to a certain state. The two conditions stated above require that in the transition matrix each column sums to 1 (that is, the total population is unchanging) and there are no negative entries (logically, populations are positive quantities). The transition matrix P is comprised of elements denoted P*ij*, relating the motion of a population from state j to state i. If the system is in current state Xi, then moves to next state Xj at the next step then it's transition probabilities is denoted as (Pij). Equation (3) is the 3 x 3 matrix represents transition probabilities between 3 different states. A given clement, p23 describes the likelihood that a member of the population will move from the state 3 to 2.

$$Pij = \begin{bmatrix} p11 & p12 & p13 \\ p21 & p22 & p23 \\ p31 & p32 & p33 \end{bmatrix} \text{.....Equation 3}$$

The basic property of a Markov chain is that only the most recent point in the trajectory affects what happens next (Ghosh *et al.*, 2017). It means that X_{t+1} depends upon X_t , but it does not depend upon X_{t-1}. . . X_1, X_0. In context of LULC dynamics, a LULC change in the Markov chain is considered as a stochastic process in which its state at a particular time t is dependent exclusively on the state at previous time step t-1 and not on the states before that – i.e., at times t-2, t-3 and so (Ghosh *et al.*, 2017). In IDRIS Selva software, Markov Chain analysis is achieved by one-click evaluation of two thematic maps collected at different period using Markov module of IDRIS Selva software (Eastman, 2012). Markov chain determines the amount of LULC change using the earlier and later LULC thematic maps and generates a transition probability matrix, a transition areas matrix and a set of conditional probability images (Eastman, 2012). The transition probability matrix is a text file containing the probability of each LULC category to change to other LULC category while transition areas matrix is a text file containing number of pixels which are expected to change from each LULC type to other LULC category (Ghosh *et al.*, 2017).

While the development of Cellular Automation (CA) systems was attributed to Stanislaw Ulam and John von Neumann working at Los Alamos laboratory in New Mexico (Ghosh *et al.*, 2017). CA underlies dynamics of the change events based on proximity concept so that the regions closer to existing areas of the same class are more probable to change to a different class (Memarian *et al.*, 2012). A cellular automaton is a cellular entity that independently varies its condition based on its previous state (according to a Markov transition rule) and adjacent neighbors (Eastman, 2012). In general, CA is a collection of cells, of an arbitrary shape, arranged in a grid-like structure. These cells can hold different values from time to time - binary being the simplest of the forms. All the cells change their states simultaneously, i.e., at the same time according to some rule - which may be fixed at the beginning or may vary from time to time (Ghosh *et al.*, 2017). In the context of LULC dynamics, CA model is a practical tool commonly reported its application in urban system simulations (Al-sharif & Pradhan, 2013). In cells of the cellular lattice, LULC dynamics can be effectively simulated by using proper neighbourhoods of cells on the cellular grid (Putra, 2017). Therefore, the hybrid CA-Markov

ISSN No:-2456-2165

model was developed to address the shortcomings of the Markov analysis which lacks spatial characteristics. In the CA -Markov the advantages of Markov chain provides estimation and the CA adds to spatial characteristics of estimation produced (Behera *et al.*, 2012; Hyandye & Martz, 2017). Previous research work by Megahed *et al.* (2015); Estes & Loveland (1999) have described the role of Markov chain in CA-Markov model is to manage temporal dynamics among the LULC categories based on transition probabilities while CA model adds spatial characteristics basing on cellular automata spatial filter or transition potential maps (Rwanga & Ndambuki, 1991).

On the other hand, Landsat satellites have continuously acquired space-based images of the Earth's land surface, providing data that serve as valuable resources for land use/land change research since 1972 (USGS, 2016) and provide good source of input data for LCM and CA-Markov model. The launch of the Earth Resources Technology Satellite (ERTS-1), which was later renamed Landsat 1 and subsequently launches of Landsat 2, Landsat 3, and Landsat 4 in year 1975, 1978, and 1982, respectively (USGS, 2016; Phiri & Morgenroth, 2017). According to USGS (2016) the Landsat 5 launched in 1984 and continued to deliver high quality, global data of Earth's land surfaces for 28 years and 10 months while Landsat 6 failed to achieve orbit in 1993. Landsat 7 successfully launched in 1999 and continues to provide global data. Landsat 8, launched in 2013, continues the mission, and Landsat 9 is tentatively planned to launch in 2020. The evolution of Landsat mission was accompanied by in by improvement in number of bands and spatial resolution from Landsat MSS, TM, ETM and Landsat 8 while been supported by advancement in computer technology, development of geographic information systems (GIS) (Phiri & Morgenroth, 2017). Figure (1) is the timeline and history of the Landsat missions since 1972.

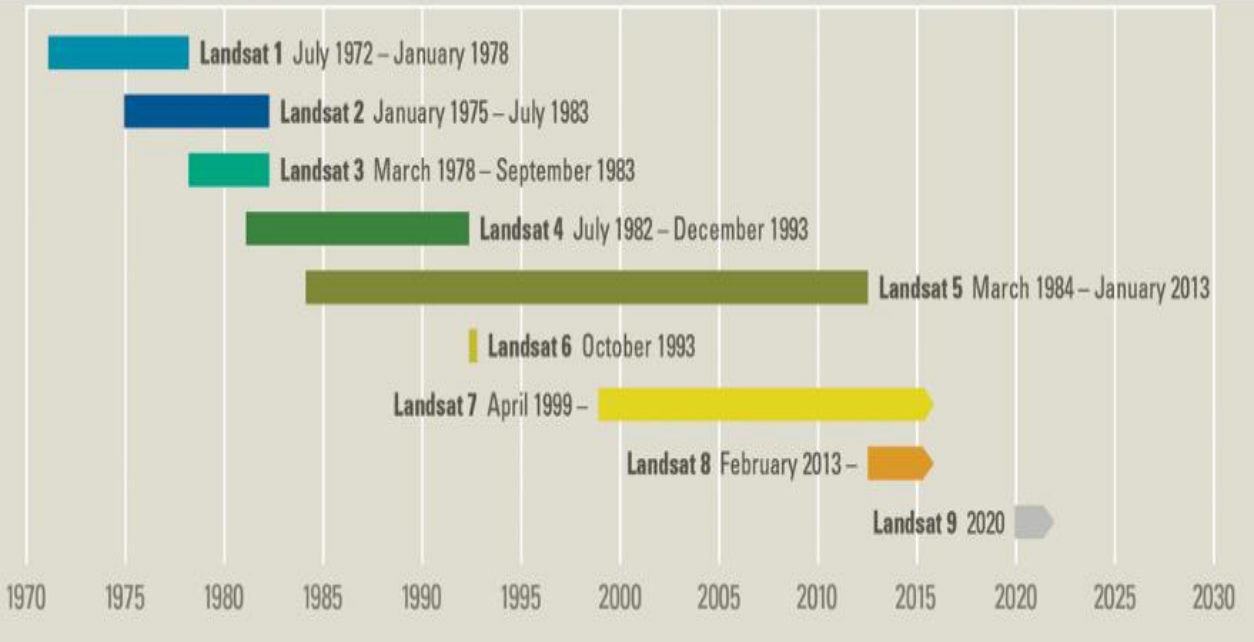

Fig 1:- Timeline and history of the Landsat Missions (USGS, 2016)

➢ *Sensors and Band Designations*

The primary sensor onboard of Landsat 1, 2, and 3 was the Multispectral Scanner (MSS), which collected data at a resolution of 79 meters and resampled to 60 meters resolution in four spectral bands ranging from the visible green to the near-infrared (IR) wavelengths. The Return Beam Vidicon (RBV) instruments on Landsat 1, 2, and 3 acquired data at 40-meter resolution, and were recorded to 70-millimeter black and white film. RVB data are archived at the Earth Resources Observation and Science (USGS 2016). Landsat 4 and Landsat 5 carried the MSS and Thematic Mapper (TM) sensor (Young *et al.*, 2017) with additional bands in shortwave infrared with improved spatial resolution of 30 meters for the visible, near-IR, and SWIR bands; and the addition of a 120-meter thermal IR band (Landgrebe, 1997). On the other hand, Landsat 7 carries the Enhanced Thematic Mapper Plus (ETM+), with 30-meter visible, near-IR, and SWIR bands; a 60-meter thermal band; and a 15-meter panchromatic band (USGS, 2016). However, on May 31, 2003, unusual artifacts began to appear within the data collected by the ETM+ instrument and investigations revealed that the Scan Line Corrector (SLC), which compensates for the forward motion of the satellite to align forward and reverse scans necessary to create an image had failed (USGS, 2016). SLC failure resulted into gaps in the captured Landsat 7 ETM+ data which formed an alternating wedge that increase in width from the centre to the edge of the image. Landsat 8, launched on February 11, 2013 as the

ISSN No:-2456-2165

Landsat Data Continuity Mission carrying the push-broom Operational Land Imager (OLI) and the Thermal Infrared Sensor (TIRS) (Young *et al.*, 2017). OLI collects data with a spatial resolution of 30 meters in the visible, near-IR, and SWIR wavelength regions, and a 15-meter panchromatic band, which provides data compatible with other previous Landsat missions (Landgrebe, 1997).

Moreover, OLI consists of a deep blue band for coastal-aerosol studies and a cirrus band for cloud detection (USGS, 2016). Furthermore, the TIRS contains two thermal bands which were designed for split-window surface temperature (USGS, 2016). Table (1) is the display and comparison of the bands and wavelengths of each Landsat sensor. For the purpose of this research study and detail required, the spectral and temporal resolutions of Landsat 5 Thematic Mapper (TM) and 8 were found appropriate for the assessments. In this research study Landsat 5 TM and Landsat 8 were selected following its good spectral bands at spatial resolution of 30 meters and temporal resolution of 16 days (Bruce & Hilbert, 2004).Landsat 5 TM data have long history and reliability hence regarded as the popular source for documenting changes in land cover and use over time (Reis et al., 2003) while Landsat facilitates documenting the current LULC categories. Table (1) details the comparison of the bands and wavelengths of each Landsat sensor.

Band designation	Landsat band wavelength comparison (all bands 30-meter resolution unless noted)									
	L8 OLI/TIRS		L7ETM+		L4-5TM		L4-5MSS		L1-3MSS	
Coastal/Aerosol	Band1	0.43-0.45	-----	----------	------	---------	------	------	--------	---------
Blue	Band2	0.45-0.51	Band1	0.45-0.52	Band1	0.45-0.52	--------	------	--------	---------
Green	Band3	0.53-0.59	Band2	0.52-0.60	Band2	0.52-0.60	Band1	0.5-0.6*	Band4	0.5-0.6*
Panchromatic	Band8**	0.50-0.68	Band8**	0.52-0.90	--------	---------		------	--------	------
Red	Band4	0.64-0.67	Band3	0.63-0.69	Band3	0.63-0.69	Band2	0.77-0.80*	Band5	0.6-0.7*
Near-Infrared	Band5	0.85-0.88	Band4	0.77-0.90	Band4	0.76-0.90	Band3		Band6	0.7-0.8*
Near-Infrared	--------	---------	-----	---------	--------		Band4	0.8-0.77*	Band7	0.8-0.11*
Citrus	Band9	1.36-1.38	-----	----------	--------					
Shortwave-Infrared-1	Band6	1.57-1.65	Band5	1.55-1.75	Band5	1.55-1.75				
Shortwave-Infrared-2	Band7	2.11-2.29	Band7	2.09-2.35	Band7	2.08-2.35				
Thermal	Band10	10.60-11.19	Band6	10.60-11.19	Band6	10.40-12.50				
Thermal	Band11	11.50-12.51	------	---------	Band3	0.63-0.69				

*=Acquired at 79 m, resampled to 60 m

**= 15 m (panchromatic)

Table 1:- Display and comparison of the bands and wavelengths of each Landsat sensor
Source: USGS (2016)

II. METHODOLOGY

A. Description and geographical locations and of study area

The Rufiji delta is located on the Rufiji basin situated between Longitudes 33º55'E and 39º25'E and between Latitudes 5º35'S and 10º45'S. The Rufuji delta is formed by the confluence of the Kilombero and the Luwegu rivers; it flows for about 175 mi northeast and east to enter the Indian Ocean, opposite Mafia Island. The river has major potential for irrigation and hydroelectric power development. Its principal tributary is the Great Ruaha. From its start at the confluence of the Kilombero and Luwegu rivers, the Rufiji flows for about 100 km to the Pangani Rapids at the entrance of the Stiegler's Gorge, where the river cut through a low ridge, forming a steep-sided narrow gorge, about 8 km long. The general flow direction of the river is from west towards east. Furthermore, the Rufiji delta is characterised as mangrove wetlands.

The Rufiji Delta covers 53,255 ha and forms part of the Rufiji River basin which extends for some 177,000 km2 (RUB ADA, 1981a) (Figure 1). As a result of deposition of sediment carried by the Rufiji River towards the coast, the shoreline has shifted seaward and presently protrudes some 15 km into the Mafia Channel. During floods, silt laden Rufiji waters penetrate far into the delta and deposit river sediments, especially along the most active deltaic branches. The estuary and delta of the Rufiji River seem to be in a state of dynamic equilibrium. The geometry and the course of the several tidal branches changes continuously by sediment deposition and erosion. The morphological conditions are disturbed by changing hydraulic features, such as fluctuating discharges, varying intrusion of salinity, and changes in sediment transport.

B. Data collection and analysis

To gain better understanding on the previous and current impacts LULC and climate changes in water resources of Rufiji delta, the Landsat data captured by multispectral sensor with moderate spatial resolution of 30 meters and temporal resolution of 16 days (Bruce & Hilbert, 2004) were used in this research study. Landsat 5 TM data and Landsat 8 data with history and reliability in capturing Earth information and documenting changes Earth ecosystems (Reis, 2008) were used in this research study.

➢ *Landsat data collection:*

The Level 1 Terrain (Corrected) Product (L1TP) of Landsat 5 TM of year 1998, 2008 and 2018 was downloaded from United State Geological Survey (USGS) official web site (http://www.earthexplore.usgs.gov.com). The Landsat data were subjected to visual assessment of the percentage cloud cover d and images of cloud cover of less or equal to 20% were found appropriate and were downloaded for the purpose of this research study. **Error! Reference source not found.** presents the Landsat dataset collected for this study.

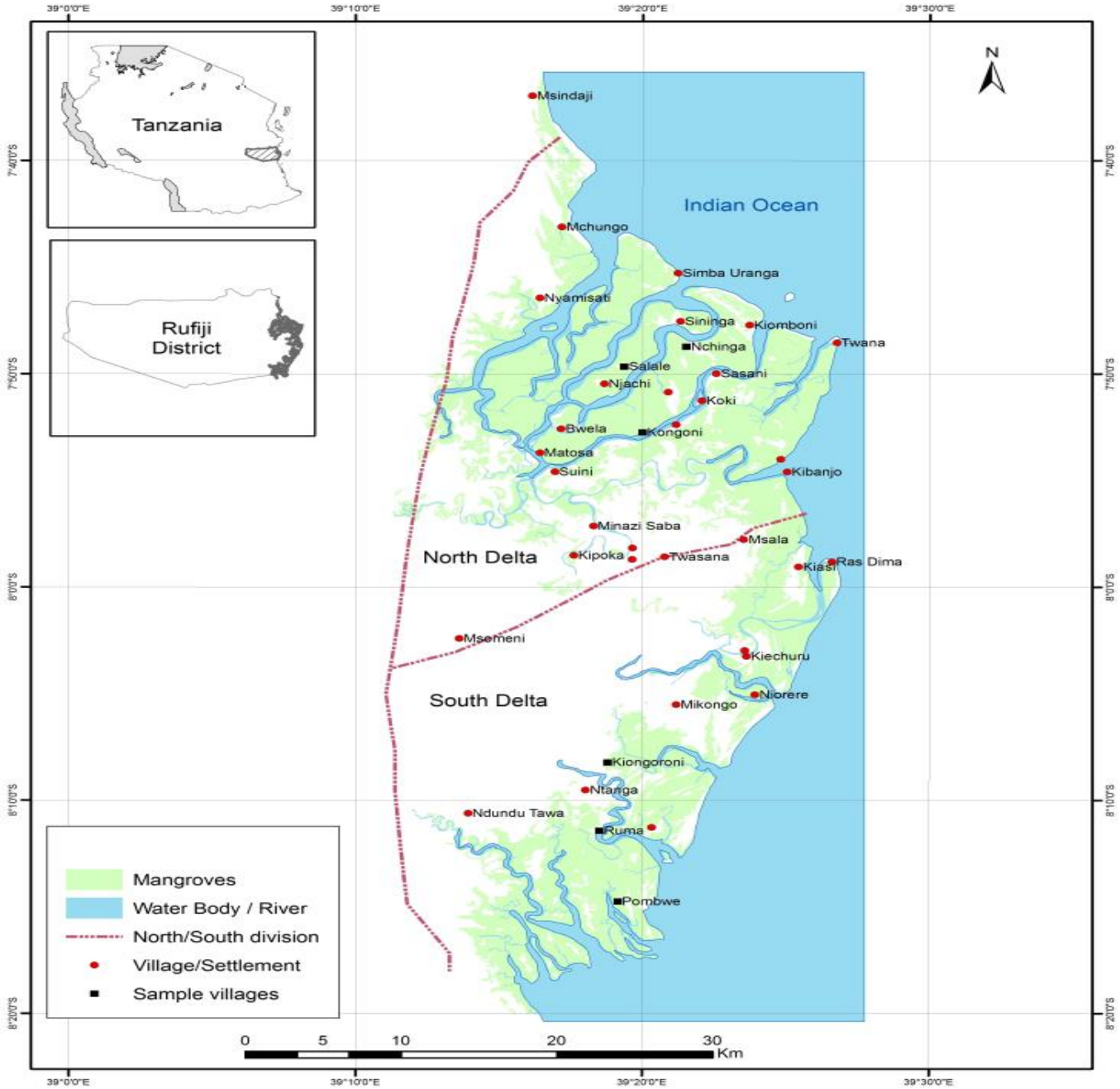

Fig 2:- Geographical location of Rufiji Delta (Source: Mwansasu, 2016)

ISSN No:-2456-2165

Dataset	Path and row	Date acquired
Landsat 5 TM	P166r65	1998-06-17
Landsat 5 TM	P166r65	2008-06-20
Landsat 8	P167r65	2018-05-3

Table 2:- Landsat dataset collected for this study
Source : (United State Geological Survey Website)

➢ *Image processing*

- *Conversion of digital numbers (DN) into reflectance:*

The conversion of digital numbers (DN) into reflectance was carried to normalize the Landsat datasets for better comparisons between images of different years of research study. The conversion involved two different steps that were carried out using ArcGIS 10.3 software. In the first step the digital number (DN) values of each pixel was converted into the radiance while the second step involved conversion of radiance into reflectance.

- *Layer stacking and image Mosaicking:*

Band 2, 3 and 4 of Landsat 5 TM images of year 1998, 2008 and 2018 from path and row of 166065 were layer stacked using ERDAS Imagine software. While the band 3, 4 and 5 of Landsat 8 of year 2018 from path and row of 166065 were layer stacked using ERDAS Imagine software. In Landsat 5 TM data, the band 6 were excluded due to its spatial resolution of 120 M while in Landsat 8 the band 6,8,10 and 11 were excluded as it possess the spatial resolution of 60, 15 and 100 M , respectively.

- *Image sub-setting:*

This was done to extract the Area of Interest (AOI) using ERDAS Imagine software. The shape file of Rufiji delata was created and used to extract the Rufiji Delta from Landsat 5 TM of year 1998, 2008 and Landsat 8 of year 2018.

- *Delineation of training sites in Landsat 5 TM and Landsat 8:*

The sub-set image of Landsat 5 TM of year 1998, 2008 and 2018 each were separately subjected to visual assessment using three bands that were displayed as Red, Blue and Green (RGB) color composite using ERDAS Imagine software. The RGB color composites images were developed to facilitate visualization, interpretation and delineation of training sites. Band 4, 3 and 2 were used in displaying in RGB color composites images for Landsat 5 TM of year 1998, 2008 and 2018. While the band 5, 4 and 3 were used in displaying in RGB color composites images for of Landsat 8 of year 2018. The training sites were delineated following the classification scheme level II by Anderson et al., (1976) with some modification. Thus in this research study only four classes which are mangrove forest, non-mangrove vegetation, water bodies and impervious LULC class were considered during image classification. Table (2) narrates the classification scheme for this research study. Delineation of training sites comprised of selecting the training sites based on visual interpretation on the image, knowledge of LULC types identified and information visualized in Google earth images. At least 20 samples of training site were developed for each identified LULC class based on the LULC type been numerous, representative, relatively homogeneous and as large as possible while maintaining homogeneity and avoiding mixed pixels at the edges of objects. Finally, the 20 samples selected for each LULC class were merged using signature editor of ERDAS Imagine to form one class.

S/N	LULC CLASS	DESCRIPTIONS
1	Mangrove forest	Forest class was formed by trees at least 5m high and canopy cover more than 50%, it comprise of deciduous, evergreen land and mixed forest.
2	Impervious	This comprised of residential places, commercial and services, industrial, transportation, communication and utilities, industrial and commercial complexes. Impervious land use also comprised of sandy areas, bare exposed rock, strip mines, quarries, and gravel pit, mixed barren land.
3	Water bodies	This comprised of water bodies comprised of rivers, streams, flooded lands and ponds
4	Non-mangrove vegetation	This comprised of vegetation other than forest class was formed by trees at least 5m high and canopy cover more than 50%, it comprise of deciduous, evergreen land and mixed forest

Table 3:- Classification scheme proposed for the research study.
Source: (Modified from Anderson *et al.*, 2001

- *Classification, post classification and accuracy assessment of Landsat dataset:*

The ERDAS Imagine software was used for classification of Landsat dataset for year 1998, 2008 and 2018 covering the Rufiji delta. Maximum Likelihood Classification (MLC) algorithm was used to develop classified images of year ear 1998, 2008 and 2018 using the signature files of Landsat image of year ear 1998, 2008 and 2018, respectively.

- *Quantification of the LULC changes for epoch of year 1998 to 2018:*

The LCM of Idris Selva software was used for change detection procedure and quantification of the LULC changes

for epoch of year 1998 to 2018. A pair wise comparison of classified images of year 1998-2008; 2008-2018; 1998-2018 were used for developing graph of gains, loss and net change of LULC categories. The LCM of IDRISI Selva software generated the graph of gain and loss as well as the graph of net change of each LULC categories for period between years of 20 years in total. While the graph of net change by LULC was constructed by taking the earlier LULC areas, adding the gains and then subtracting the losses was also constructed using IDRISI Selva.

The procedure of generating predicted LULC map using CA-Markov was divided into Markov analysis and CA-Markov modelling. In first, the Markov analysis was used for creating transition probability matrix, a transition areas matrix, and a set of conditional probability images which was achieved through pair wise comparison of LULC map of 1996 vs. 2007, 1996 vs. 2007 and 2007vs. The CA-Markov module combines the CA, Markov Chain, Multi-Criteria/Multi Objective Land Allocation (MOLA) in prediction procedure. Besides, the procedure of generating predicted LULC map using CA-Markov was divided into Markov analysis and CA-Markov modelling. In first, the Markov analysis was used for creating transition probability matrix, a transition areas matrix, and a set of conditional probability images which was achieved through pair wise comparison of LULC map of 1996 vs. 2007, 1996 vs. 2007 and 2007vs. 2018. A pair wise comparison LULC map of 1996 vs. 2007 using Markov tool in IDRIS Selva, the transition probability matrix, a transition areas matrix, and a set of conditional probability images from year 2007 to 208 were created and used for simulating and predicting the LULC in year 2018. On the other hand, LULC of year 2007 and 2018 were used to create the transition probability matrix, a transition areas matrix, and a set of conditional probability images from year 208-2048 which was used for predicting the LULC in year 2048.

- *Model validation :*

The validity of the CA-Markov were assessed using these following statistics which are the Kappa Index of Agreement (KIA) denoted as Kstandard; Kappa for no information (denoted Kno); Kappa for grid-cell level location (denoted Klocation) and Kappa for stratum-level location (denoted KlocationStrata). These statistics were generated using VALIDATE module in IDRIS Selva. In VALIDATE module, the predicted LULC map of year 2018 was used as comparison data while and the classified map of year 2018 used as reference data in validating the CA-Markov model results. The VALIDATE module generated statistic for validation which was KIA, Kno; Klocation and Kappa KlocationStrata. When results of each validation static scores at least 85%, the model was considered worth for next step which consisted simulating LULC category of year 2048.

III. RESULTS AND DISCUSION

A. LULC classification results

The classification results of four different study periods have depicted the quantity land use land cover status in year 1998, 2008 and 2018. Four LULC classes classified were mangrove forest, non- mangrove forest, water bodies and impervious. Using **Error! Reference source not found.** in year 1998 the impervious land cover was the largest class with 53413.40 ha (35.74% composition), followed by water bodies with 42506.10 ha (28.44% composition) while mangrove forest and non-mangrove vegetation consisted of 38060.40 ha (25.47 % composition) and 15468.50 ha (10.35% composition), correspondingly. In year 2008, the impervious land cover was the largest class with 61977.00 ha (41.47 % composition), followed by Mangrove forest with 36646.20 ha (24.52% composition) while water bodies decline to 31519.40 ha (21.09% composition). Moreover, the non-mangrove vegetation and water bodies declined to 19305.50 ha (12.92 % composition) and 31519.40 ha (21.09 % composition), correspondingly. In year 2018 the impervious land cover increased to 60759.70 ha (40.66% composition) while mangrove forest and non-mangrove vegetation consisted of 35062.2 ha (23.46% composition) and 23019.2 ha (15.40% composition), correspondingly. Water bodies declined to 30607.10 ha (20.48% composition) following the consumption of water in hydro-electrical and agricultural expansion proximal to the Rufiji Delta.

B. Results of Markov model

The first-order Markov probability was obtained using LULC map of year 1998-2008, 2008-2018 and 1998- 2018 (**Error! Reference source not found.**5-7). Transition probability matrix generated was used to portray the likelihood of each LULC category to change into other LULC category from 1998-2008, 2008-2018 and 1998- 2018 (**Error! Reference source not found.**5-7). In both periods the transition probability of LULC category did not remain unchanged, there was both dynamism of mangrove forest, non- mangrove forest, water bodies and impervious for this research study.

- *Mangrove forest:*

In year 1998 to 2008 the chance of mangrove remaining unchanged was 0.45 (45%) while the probability of changing to non-mangrove vegetation, impervious and water bodies was 0.099 (9%), 0.40 (40%) and 0.06 (6%), correspondingly. The high probability of mangrove forest changing to impervious land cover is supported by previous research reports which have demonstrated the presence of illegal harvesting of mangrove forest for both construction and local use. In year 2008 to 2018 the probability of mangrove forest remaining unchanged increased to 0.51 (51%) while the probability of changing to non-mangrove vegetation, impervious and water bodies was 0.10 (10%), 0.34 (34%) and 0.04 (4%). The low chance of mangrove changing into

ISSN No:-2456-2165

impervious land cover decreased from year 2008 to 2018 following the interception of Ramsar Convention in 2000s which have encouraged protection of Rufiji mangrove forests. On the other hand, in year 2008 to 2018 the chance of mangrove forest changing into non-mangrove vegetation, impervious and water bodies was 0.099 (9%), 0.3965 (39%) and 0.057 (5%) respectively. However, the chance of remaining unchanged was reduced to 0.4479 (44%). In year 1998 to 2018 the probability of mangrove forest remaining unchanged increased to 0.51 (51%) while the probability of changing to non-mangrove vegetation, impervious and water bodies was 0.10 (10%), 0.34 (34%) and 0.04 (4%).

- *Non-mangrove vegetation:*

In year 1998 to 2008 the chance of non- mangrove vegetation remaining unchanged was 0.3197 (31%) while the probability of changing to mangrove forest, water bodies and impervious was 0.2704 (27%) 0.0670 (6%) and 0.5022 (50%), respectively. On contrary in year 2008 to 2018, the chance of non- mangrove vegetation remaining unchanged was 0.2795 (27%) while the probability of changing to mangrove forest, water bodies and impervious was 0.4531 (43%) 0.0926 (0.092%) and 0.1749 (17%), respectively. %). In year 1998 to 2018 the probability of non-mangrove vegetation remaining unchanged increased to 0.51 (51%) while the probability of changing to non-mangrove vegetation, impervious and water bodies was 0.10 (10%), 0.34 (34%) and 0.04 (4%).

- *Water bodies:*

In year 1998 to 2008 the chance of water remaining unchanged was 0.7990 (79%) while the probability of changing to non-mangrove vegetation, impervious and mangrove was 0.0546 (5%), 0.0946 (9%) and 0.0518 (5%), respectively. On contrary in year 2008 to 2018, the chance of remaining unchanged was 0.7557 (75%) while the probability of changing to non-mangrove vegetation, impervious and mangrove was 0.1216 (12%), 0.0794 (7%) and 0.0434 (4%), respectively. In year 1998 to 2018, the chance of remaining unchanged was 0.8430 (84%) while the probability of changing to non-mangrove vegetation, impervious and mangrove was 0.0665 (6%), 0.0528 (5%) and 0.0377 (4%), respectively.

- *Impervious:*

In year 1998 to 2008 the chance of impervious remaining unchanged was 0.5280 (52%) while the probability of changing to non-mangrove vegetation, water and mangrove was 0.1829 (18%), 0.0396 (3%) and 0.2495 (24%), respectively. On contrary in year 2008 to 2018, the chance of remaining unchanged was 0.5280 (52%) while the probability of changing to non-mangrove vegetation, water and mangrove was 0.1829 (18%), 0.0396 (3%) and 0.2495 (24%), respectively. In year 1998 to 2018, the chance of remaining unchanged was 0.5721 (57%) while the probability of changing to non-mangrove vegetation, water and mangrove was 0.1370 (13%), 0.0131 (1%) and 0.2778 (27%), respectively.

LULC category	Area (ha) in year 1998	% composition	Area (ha) in year 2008	% composition	Area in year 2018	% composition
Water bodies	42506.10	28.44	31519.40	21.09	30607.1	20.48
Mangrove forest	38060.40	25.47	36646.20	24.52	35062.2	23.46
Impervious	53413.40	35.74	61977.00	41.47	60759.7	40.66
Non-mangrove	15468.50	10.35	19305.50	12.92	23019.2	15.40
TOTAL	**149448.40**	**100.00**	**149448.10**	**100.00**	**149448.20**	**100.00**

Table 4:- Area of LULC categories in (ha) and % composition for year 1998, 2008 and 2018

ISSN No:-2456-2165

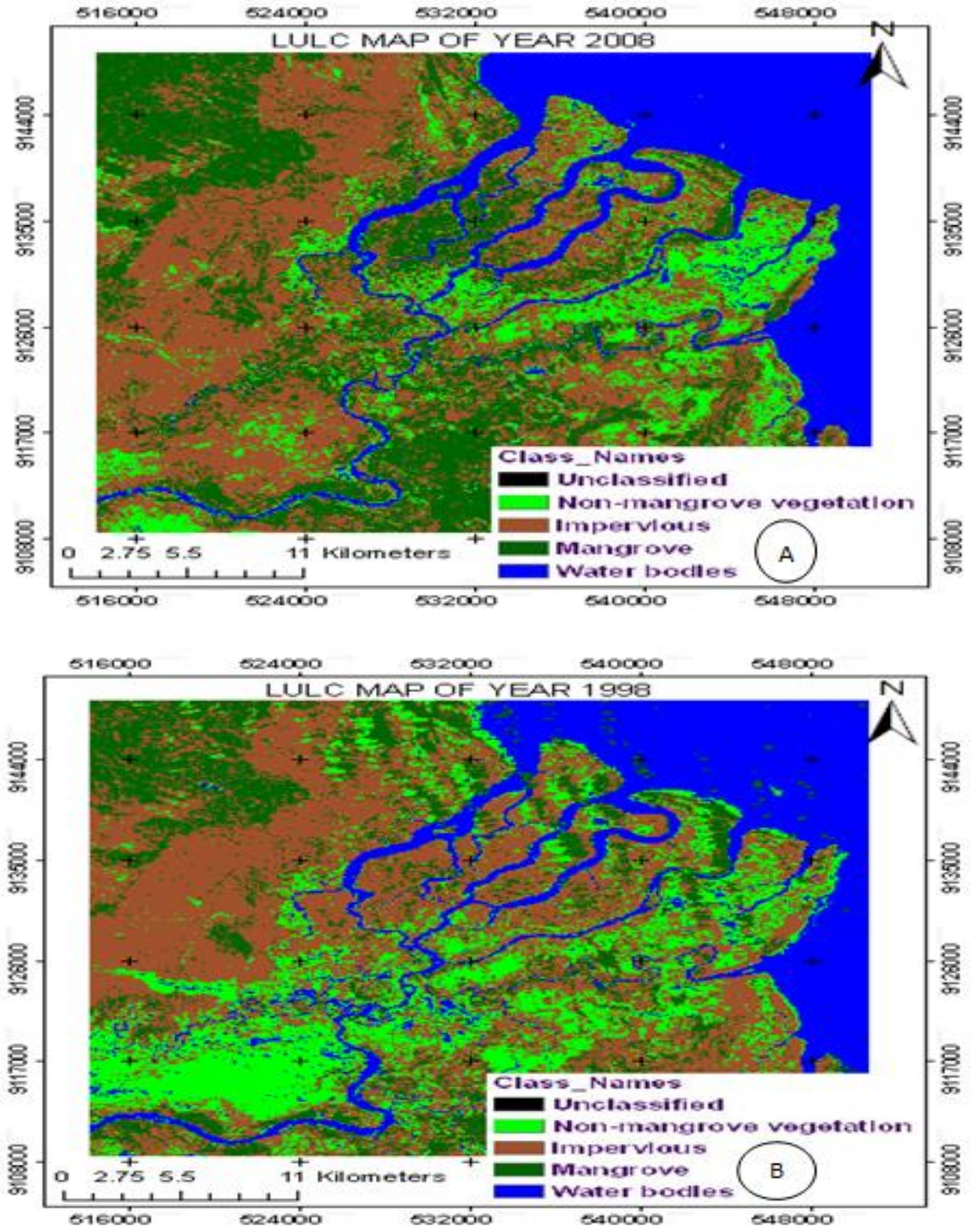

Fig 3:- LULC map of year 1998 and 2008 in "A" and "B", correspondingly.

ISSN No:-2456-2165

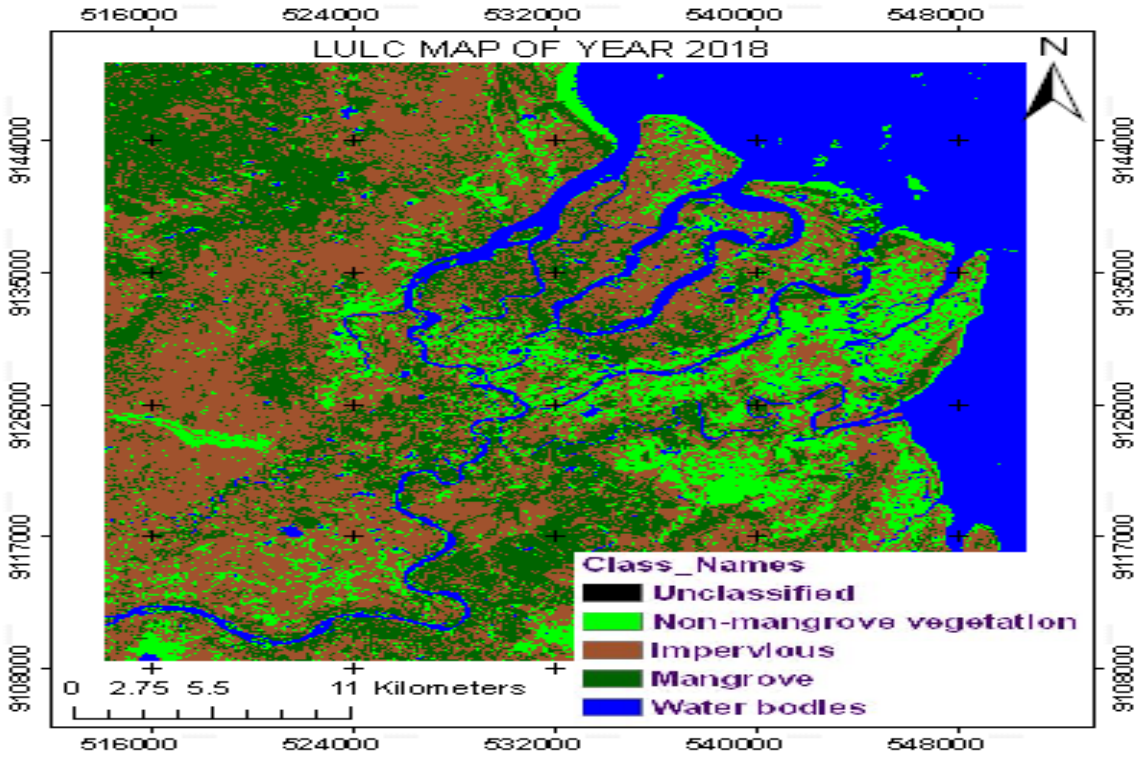

Fig 4:- LULC map of year 2018

LULC Category	Non-mangrove	Impervious	Water bodies	Mangrove forest
Non-mangrove vegetation	0.1604	0.5022	0.0670	0.2704
Impervious	0.1227	0.4996	0.0209	0.3568
Water bodies	0.0546	0.0946	0.7990	0.0518
Mangrove forest	0.0987	0.3965	0.0568	0.4479

Table 5:- Transition probability matrix in year 1998 to 2008

LULC Category	Non-mangrove	Impervious	Water bodies	Mangrove forest
Non-mangrove vegetation	0.2795	0.4531	0.0926	0.1749
Impervious	0.1829	0.5280	0.0396	0.2495
Water bodies	0.1216	0.0794	0.7557	0.0434
Mangrove forest	0.1408	0.4600	0.0355	0.3636

Table 6:- Transition probability matrix in year 2008 to 2018

LULC Category	Non-mangrove	Impervious	Water bodies	Mangrove forest
Non-mangrove vegetation	0.3197	0.4867	0.0461	0.1475
Impervious	0.1370	0.5721	0.0131	0.2778
Water bodies	0.0665	0.0528	0.8430	0.0377
Mangrove forest	0.1039	0.3415	0.0439	0.5107

Table 7:- Transition probability matrix in year 1998 to 2018

C. CA-Markov results

➢ *Predicted LULC in 2048*

In year 2048 a notable decline to about 29757.07 ha, (18.91%), 34891.44 ha (21.35were recorded for mangrove forest and water bodies, correspondingly. The ongoing harvesting and clearing of mangrove forest for construction and other local use purpose (Wagner *et al.*, 2003 & Shapiro *et al.*, 2015) if will persist for 30 years, the recorded decline trends will be evident in Rufiji Delta. While the decline in water bodies are likely to occur following the extended use for domestic, agricultural and hydro-power generation couple with the expended decrease following the impacts in hydrological circle (Wagner et al., 2003). Effort to manage the future situation will include development and management of water shades proximal to Rufiji Delta as well as promoting agricultural technology that uses small quantity of water.

On the other hand, substantial increase in area non-mangrove vegetation and impervious was estimated to 22507.20 ha and 62292.84 ha, correspondingly. The expected increase in non-mangrove vegetation is resulting from expansion following the increase in human population which depends on agriculture as main economic activities. While the increasing dryness of land surface following the deforestation of mangrove vegetation couple with expansion of settlements accounts for the expected increase in area under impervious land cover in year 2048.

LULC Category	Area (ha) in year 2048	% composition
Non-mangrove vegetation	22507.20	18.06
Impervious	62292.84	42.68
Water bodies	29757.07	18.91
Mangrove forest	34891.44	21.35
TOTAL	**149448.1**	**100.00**

Table 8:- Simulated LULC category for year 2048

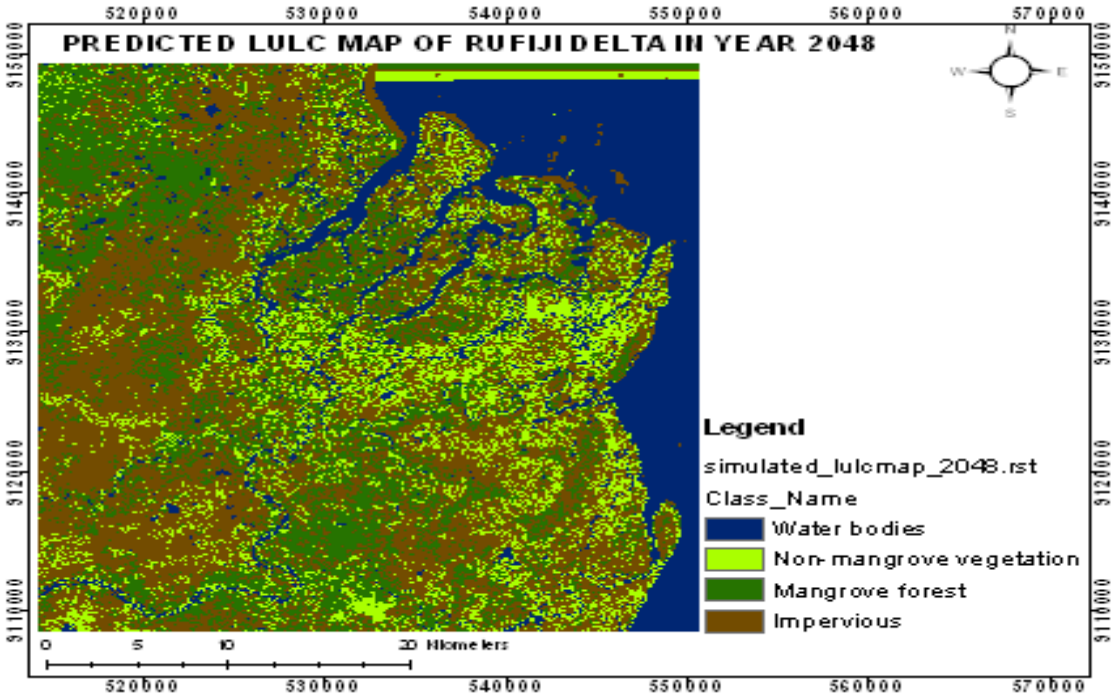

Fig 5:- Simulated LULC categories in year 2048

IV. CONCLUSION AND RECOMMENDATION

This research generated past, present and future LULC information using Landsat data and CA-Markov model, correspondingly. The past and present LULC information generated through classification the Landsat 5 TM of year 1998, 2008 and Landsat 8 of 2018 using ERDAS Imagine software. The CA-Markov model was used to generate the future states of LULC in Rufiji Delta. The Landsat classification and CA-Markov model have both indicated the capability in appraising and simulating the past, present and future LULC dynamics in Rufiji Delta. Basing on the findings of this research mangrove forest and water bodies will continue to decrease while the impervious and non-mangrove vegetation will increase in 30 years to come. For sustainability of resources around the Rufiji Delta, afforestation, agro-forestry and watershed management is highly recommended in Rufiji Delta.

V. REFERENCES

[1]. Araya, Y. H., & Cabral, P. (2010). Analysis and modeling of urban land cover change in Setúbal and Sesimbra, Portugal. *Remote Sensing*, *2*(6), 1549–1563. https://doi.org/10.3390/rs2061549

[2]. Bruce, C. M., & Hilbert, D. W. (2004). Pre-processing Methodology for Application to Landsat TM/ETM+ Imagery of the Wet Tropics. *Cooperative Research Centre for Tropical Rainforest Ecology and Management. Rainforest CRC, Cairns.*, 44 pp. https://doi.org/10.1155/2010/468147

[3]. Eastman, J. R. (2012). IDRISI Selva Tutorial. *Clark Universtity*, *Manual Ver*(January).

[4]. Ghosh, P., Mukhopadhyay, A., Chanda, A., Mondal, P., Akhand, A., Mukherjee, S., … Ghosh, T. (2017). Remote Sensing Applications : Society and Environment Application of Cellular automata and Markov-chain model in geospatial environmental modeling- A review. *Remote Sensing Applications: Society and Environment*, *5*(January), 64–77. https://doi.org/10.1016/j.rsase.2017.01.005

[5]. Hamdy, O., Zhao, S., A. Salheen, M., & Eid, Y. Y. (2017). Analyses the Driving Forces for Urban Growth by Using IDRISI®Selva Models Abouelreesh - Aswan as a Case Study. *International Journal of Engineering and Technology*, *9*(3), 226–232. https://doi.org/10.7763/IJET.2017.V9.975

[6]. Houet, T., Hubert-moy, L., Houet, T., Modeling, L. H., & States, F. (2007). Modeling and projecting land-use and land-cover changes with Cellular Automaton in considering landscape trajectories To cite this version : HAL Id : halshs-00195847 TRAJECTORIES : AN IMPROVEMENT FOR SIMULATION OF PLAUSIBLE.

[7]. Hyandye, C., & Martz, L. W. (2017). A Markovian and cellular automata land-use change predictive model of the Usangu Catchment. *International Journal of Remote Sensing*, *38*(1), 64–81. https://doi.org/10.1080/01431161.2016.1259675

[8]. Landgrebe, D. (1997). The Evolution of Landsat Data Analysis 1, *63*(7), 859–867.

[9]. Ma, C., Zhang, G. Y., Zhang, X. C., Zhao, Y. J., & Li, H. Y. (2012). Application of Markov model in wetland change dynamics in Tianjin Coastal Area, China. *Procedia Environmental Sciences*, *13*(2011), 252–262. https://doi.org/10.1016/j.proenv.2012.01.024

[10]. Mahmoud, M. I. (2016). Integrating Geoinformation and Socioeconomic Data for Assessing Urban Land-use Vulnerability to Potential Climate-change Impacts of Abuja By, (May).

[11]. Memarian, H., Kumar Balasundram, S., Bin Talib, J., Teh Boon Sung, C., Mohd Sood, A., & Abbaspour, K. (2012). Validation of CA-Markov for Simulation of Land Use and Cover Change in the Langat Basin, Malaysia. *Journal of Geographic Information System*, *04*(06), 542–554. https://doi.org/10.4236/jgis.2012.46059

[12]. Mirhosseini, S. M., Jamali, A. A., & Hosseini, S. Z. (2016). Investigating and Predicting the Extension of Dunes Using Land Change Modeler (LCM) in the North West of Yazd , Iran, *1*, 76–90.

[13]. Mwansasu, S. (2016). *Causes and Perceptions of Environmental Change in the Mangroves of Rufiji Delta , Tanzania Implications for Sustainable Livelihood and Conservation.*

[14]. Paul, S. S. (2013). Analysis of land use and land cover change in kiskatinaw river watershed: a remote sensing, gis & modeling approach.

[15]. Phiri, D., & Morgenroth, J. (2017). Developments in Landsat land cover classification methods: A review. *Remote Sensing*, *9*(9). https://doi.org/10.3390/rs9090967

[16]. Putra, U. (2017). APPLICATION OF CA-MARKOV MODEL AND LAND USE / LAND COVER CHANGES IN MALACCA RIVER WATERSHED , *15*(4), 605–622.

[17]. Rwanga, S. S., & Ndambuki, J. M. (1991). Accuracy Assessment of Land Use / Land Cover Classification Using Remote Sensing and GIS, *2017*, 611–622. https://doi.org/10.4236/ijg.2017.84033

[18]. Shapiro AC, Trettin CC, Küchly H, Alavinapanah S, Bandeira S (2015) The mangroves of the Zambezi Delta: Increase in extent observed via satellite from 1994 to 2013. Remote Sensing, 15 pp

[19]. USGS. (2016). Landsat – Earth observation satellites: Fact Sheet, *2020*(August 2016), 4. https://doi.org/10.3133/fs20153081

[20]. Weng, Q. (2002). Land use change analysis in the Zhujiang Delta of China using satellite remote sensing, GIS and stochastic modelling. *Journal of Environmental Management*, *64*(3), 273–284. https://doi.org/10.1006/jema.2001.0509.
[21]. Wagner G M, Sallema-Mtui R (2016) The Rufiji Estuary: Climate change, anthropogenic pressures, vulnerability assessment and adaptive management strategies. Western Indian Ocean, Estuaries of the World [DOI 10.1007/978-3-319-25370-1-12]
[22]. Yasmine Megahed *, Pedro Cabral, J. S. and M. C. (2015). Geo-Information Greater Cairo Region — Egypt, 1750–1769. https://doi.org/10.3390/ijgi4031750
[23]. Young, N. E., Anderson, R. S., Chignell, S. M., Vorster, A. G., Lawrence, R., & Evangelista, P. H. (2017). A survival guide to Landsat preprocessing. *Ecology*, *98*(4), 920–932. https://doi.org/10.1002/ecy.1730
[24]. Zhigang Cheng, & Shuangping Cao. (2011). Markov processes in modeling land use and land cover change in Tibetan Plateau. *2011 International Conference on Remote Sensing, Environment and Transportation Engineering*, *72*(158), 457–459. https://doi.org/10.1109/RSETE.2011.5964312